Available online at www.sciencedirect.com

ScienceDirect

Procedia Structural Integrity 54 (2024) 414–422

Structural Integrity Procedia

www.elsevier.com/locate/procedia

International Conference on Structural Integrity 2023 (ICSI 2023)

# The thermal influence on the material durability of additive manufactured glass fibre reinforced polymer with embedded fibre Bragg grating sensor

Magdalena Mieloszyk[a,*], Artur Andrearczyk[a], Ruta Rimasauskiene[b], Marius Rimasauskas[b], Anita Orlowska[c]

[a]*Institute of Fluid Flow Machinery, Polish Academy of Sciences, Fiszera 14, 80-231 Gdansk, Poland*
[b]*Kaunas University of Technology, Studentu 56, Kaunas 51424, Lithuania*
[c]*Institute of Fundamental Technological Research of the Polish Academy of Sciences, Pawinskiego 5B, 02-106 Warsaw, Poland*

**Abstract**

The goal of the paper is to analyse the influence of embedded fibre Bragg grating (FBG) sensors on additive manufactured (AM) glass fibre reinforced polymer (GFRP) samples structure and durability. The samples were manufactured using the modified fused deposition modelling (FDM) method. Two types of samples were fabricated (without and with FBG sensors embedded in the middle). The AM process did not influence the FBG sensors spectra shape. The sensors were applied for strain measurements during the thermal and tensile tests.

The samples (without and with embedded FBG sensors) were divided into two sets. One of them was exposed to assumed values of temperatures (in a range of 10°C to 50°C) under stable relative humidity levels (20% and 95%) in an environmental chamber. While the second set remained intact. Then the tensile test was performed on all samples to analyse the embedded FBG sensors influences on AM GFRP samples durability. Additionally, the samples structure (after manufacturing and after thermal tests) was measured using SEM microscope and THz spectrometer. The analyses allowed better understanding of the influence of the temperature on the GFRP material structure as well as the breaking process during the tensile test.

It was concluded that embedded FBG sensors can be applied for strain measurements of AM GFRP elements exposed to thermal and mechanical loading. Additionally, it was observed that the sensors influence on the material durability was neglected and the AM method can be applied to manufacturing smart structures.



*Keywords:*
Additive manufacturing; Structural Health Monitoring; fibre Bragg grating sensors

* Corresponding author.
*E-mail address:* mmieloszyk@imp.gda.pl


10.1016/j.prostr.2024.01.101

**Nomenclature**

| | |
|---|---|
| $\lambda_m$ | measured Bragg wavelength |
| $\lambda_b$ | base Bragg wavelength |
| $\epsilon_m$ | mechanical strain |
| $\epsilon_c$ | total strain |
| $\epsilon_f$ | optical fibre strain |

## 1. Introduction

Glass fibre reinforced polymers (GFRP) are nowadays very popular in a variety of structures - bridges (Sá et al. (2017)), ships (Cucinotta et al. (2017)), wind turbines (Park et al. (2011)). It is an effect of GFRP advantages like: low weight, high resistance to environmental factors and fatigue loads (Tuwair et al. (2016)). Due to this GFRP elements operate under a variety of environmental and loading conditions.

Environmental awareness results in development of new manufacturing methods that allow fabricating elements with a complex shapes and producing a limited amount of waste. Such requirements can be fulfilled by additive manufacturing (AM) techniques. Also elements from fibre reinforced polymers (FRP) can be manufactured using 3D printing techniques (Karaş et al. (2022); Dickson et al. (2017)). It is worth mentioning that structure of final product is influenced by the manufacturing method parameters. AM FRP laminate can contains voids also debonding between consecutive layers and inside layers (between neighbouring fibre reinforcements) can occurs.

Analogically, like FRP materials manufactured using standard method, AM GFRP elements are composed from two materials with different mechanical and physical properties: polymeric matrix and fibre reinforcement. Also their sensitivity on environmental parameters is different. From those two main components, the matrix is more sensitive on temperature and moisture than the reinforcement.

Elevated temperatures negatively influenced on fibres (e.g. decreasing of their strength and stiffness), bonds between fibres and matrix (e.g. reduction of adhesion in the reinforcement/ matrix connection) as well as chemical and physical changes in the polymer matrix (matrix cracking, plasticisation, etc.). The other parameter is moisture that influence affects a polymer properties (e.g. dimensional stability, mechanical, and thermophysical properties, plasticisation, glass transition temperature reduction) Eftekhari and Fatemi (2016) and the fibre-matrix interface bond (loss of mechanical integrity) Eslami et al. (2012). Without a strong bond at the interface, the properties of the weakest component (matrix), dominates in FRP structure (Eftekhari and Fatemi (2016); Eslami et al. (2012)).

Recently, FRP structures with embedded sensors are applied in many branches (e.g. marine Mieloszyk et al. (2020), civil engineering Gebremichael et al. (2005)) of industry. Such sensors are parts of structural health monitoring (SHM) systems installed of such structures. Also AM methods are developed for the purpose of manufacturing structures with embedded sensors Nagulapally et al. (2023).

One of the sensors types used in SHM systems are fibre Bragg grating (FBG) sensors Roberts et al. (2021); Feng et al. (2019). Due to their advantages (e.g. small dimensions, high corrosion resistance) they can be embedded into GFRP elements. FBG sensors are mostly applied for measurements strain Wu et al. (2019) and temperature Chen et al. (2020).

The aim of the paper is to analyse influence of elevated temperature on internal structure of GFRP samples with embedded FBG sensors. The samples were fabricated using AM. The paper is organised as follows. Firstly, used AM method and samples will be described. Then experimental investigation results will be presented and discussed. Finally, some conclusions are drawn.

## 2. Manufacturing method and samples

The analyses were performed on GFRP samples manufactured using modified fused deposition modelling (FDM) method. The manufacturing process was made using modified 3D printer (MeCreator 2) in which two separated heads

(for polymer and reinforcement) were replaced by one used for impregnated fibre. The principle of operation of the AM process is presented in Rimašauskas et al. (2019). The main parameters of the process and used materials are collected in Table 1.

Table 1. AM process parameters and used materials.

| Printing settings | Parameter |
|---|---|
| Nozzle (stainless steel) diameter | 1.5 mm |
| Extrusion multiplier | 0.8 |
| Extruder temperature | 220 °C |
| Build platform temperature | 80°C |
| Printing speed | 180 mm/min |
| Line width | 1.3 mm |
| Layer height | 0.5 mm |
| Number of layers | 4 |
| Fibre orientation | Unidirectional 0° |
| Infill ratio | 100 % |
| Matrix | polylactic acid (PLA) |
| Fibre reinforcement | continuous glass fiber (EC11 300) |
| Stacking sequence | [0,0]s |

A photograph of GFRP sample after manufacturing are presented in Figure 1. Measurements were performed on 5 samples without embedded sensors and 5 samples with embedded FBG sensors. Each sample dimensions were 150 mm x 12 mm x 2 mm. FBG sensors (10 mm gauge length) were embedded in the middle of samples (between the second and the third layer). The sensors were located parallel to the main axis of the sample and the continuous fibres directions. Photograph of the zoom of the sample structure after manufacturing is presented in Figure 2. The AM method results in structure containing attached glass fibre bundles covered by PLA polymer.

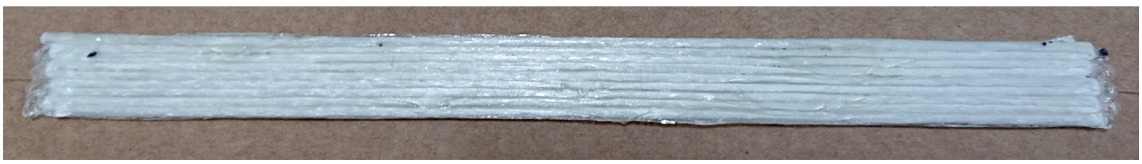

Fig. 1. Photograph of GFRP sample with embedded FBG sensor.

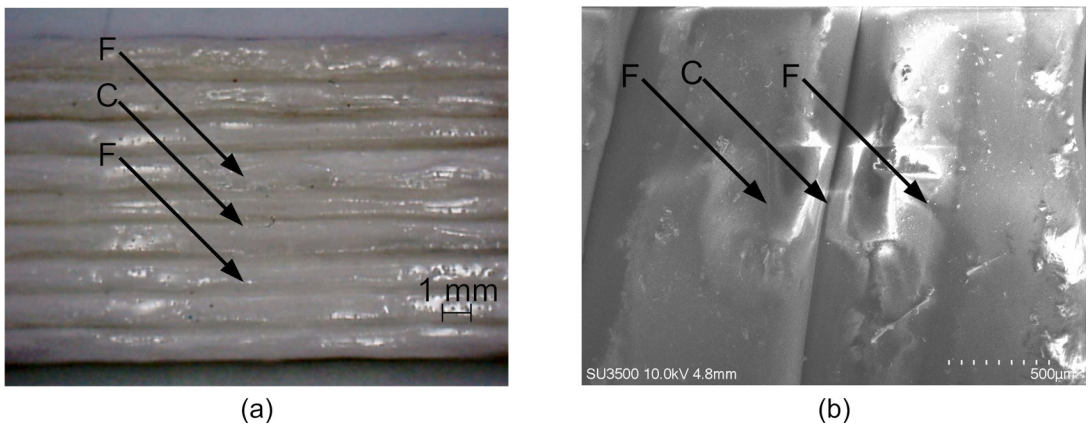


Fig. 2. Sample structure after manufacturing: (a) optical microscope, (b) SEM microscope; F – fibre bundles, C – connection.

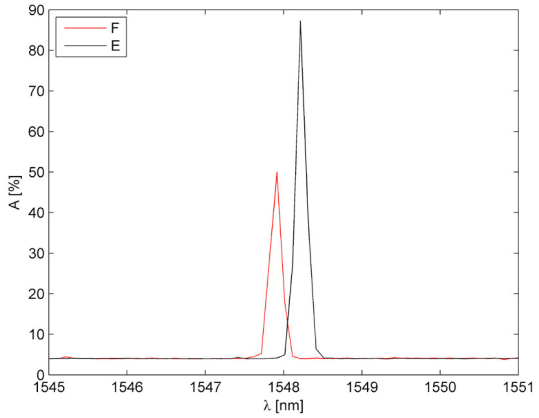


Fig. 3. A comparison of FBG sensors spectra: f – free, e – embedded.

Firstly, after the end of AM process, FBG spectra of the embedded sensors were compared with spectra of the same sensors in free conditions. For all samples the achieved results were similar. The embedding process caused sensor reflectivity reduction (ca. 50%) and remaining compression strain (ca. $4\text{x}10^{-4}$ m/m) occurrence – see comparison of FBG sensor spectra in Figure 3. Because spectra shape distortion were not observed the AM method can be applied for manufacturing elements with embedded FBG sensors.

## 3. Experimental investigation

The experimental investigation contained two main parts. The first was related to temperature loading under stable relative humidity (RH) values while in the second, the tensile test was performed on the same AM samples.

### *3.1. Thermal loading*

The measurements of the elevated temperature influence was performed in environmental chamber MyDiscovery DM600C (Angelantoni Test Technologies Srl, Italy). The samples were exposed to nine temperature values from a range of 10°C to 50°C with a step of 5°C. The investigations were performed under stable relative humidity (RH) level equal to 20% and 95%. The aim of the investigation was to determine the influence of moisture and temperature on AM GFRP material.

During the test, 5 samples of each type (without and with embedded FBG sensors) were kept on a lattice shelf to allow them expanding in all directions. The measurements were performed using interrogator si425-500 from Micron Optics with a measurement frequency equal to 1 Hz.

For the purpose of determining the mechanical strain in the samples a following procedure was performed. Firstly, total strain $varepsilon_c$ values measured by FBG sensors were calculated. It contains thermal influence on FBG sensor and the fibre optic material that is ca. 10 times higher than mechanical strain influence Mieloszyk et al. (2020). For calculating $varepsilon_c$ the following equation was used

$$\varepsilon_c(T, RH) = \frac{\lambda_m(T, RH) - \lambda_b(T)}{\lambda_b(T, RH)} \tag{1}$$

where $\lambda_m$ and $\lambda_b$ are measured and base Bragg wavelengths, respectively. The base condition temperature was equal to 20°C and RH level was 20%.

Then the mechanical strain in the GFRP material was determined using the following relationship:

$$\varepsilon_m(T, RH) = \varepsilon_c(T, RH) - \varepsilon_f(T, RH) \tag{2}$$

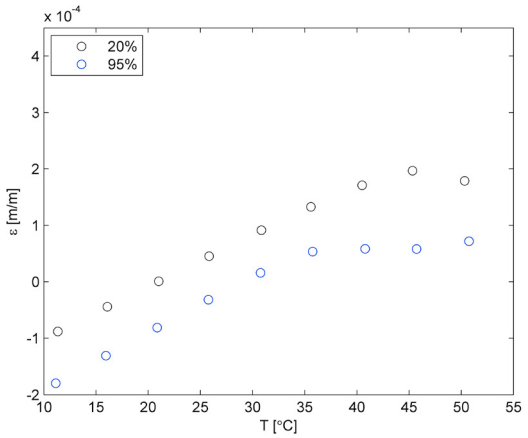


Fig. 4. A comparison of thermal strain values for two RH values.

where $\varepsilon_f$ is strain determined experimentally for free FBG sensor exposed to temperature under 20% and 95% RH levels.

The mean strain values for embedded FBG sensors from all samples for both RH values are presented in Figure 4. The absolute strain values differences were equal to $3x10^{-6}$ [m/m].

For both RH values, strain increases up to maximal value and then decrease (for 20% RH) or is almost stable (for 95% RH). Glass transition temperature of PLA lies between 50°C and 70°C Cristea et al. (2020). PLA is a semi-crystalline type of polymer. Additionally, the polymer structure of PLA is cross-linked, which means that it may not be easily degraded.The procedure of preparation glass fibres before printing process influenced cross-lining. It results in lower glass transition temperature of PLA matrix. The details of the observed phenomena for FRP material manufactured using the same AM method were described in Muna and Mieloszyk (2021). The presented values shows also the influence of RH on PLA material – lowering of the glass transition temperature due to moisture diffusion into material structure. It also results in lower strain values for all analysed temperatures.

Table 2. Comparison of strain values and coefficient of thermal expansion (CTE) for two RH values.

| Parameters | 20% RH | 95% RH |
|---|---|---|
| Maximal strain [mm/mm] | $20.1x10^{-5}$ (at 45°C) | $5.9x10^{-5}$ (at 40°C) |
| Strain [mm/mm] at 10°C | $-9.5x10^{-5}$ | $-18.0x10^{-5}$ |
| Strain [mm/mm] at 50°C | $18.2x10^{-5}$ | $7.2x10^{-5}$ |
| CTE [1/°C] | $8.88x10^{-6}$ | $9.47x10^{-6}$ |

A comparison of strain values for three chosen temperatures and coefficient of thermal expansion (CTE) for both RH values are presented in Table 2. For both cases the CTE values were determined for the linear part of relationship between strain and temperature – from 10°C to temperature for the maximal strain. CTE values for GFRP material manufactured using standard production methods are in the range of $5.4x10^{-6}$ 1/°C to $9.1x10^{-6}$ 1/°C Vaggar et al. (2018). The CTE values for AM GFRP material are close to the maximal value of the presented range. Also here the RH influence is observable as increasing of CTE value for 6%.

### *3.2. THz spectroscopy*

Samples after manufacturing and then after thermal loading under selected stable RH values, were examined using THz spectroscopy. It is one of non-destructive methods that based on electromagnetic waves (typically 0.1 – 10 THz) and can be applied for non-conductive materials. The method can be applied for detection and localisation of defects

like voids Stoik et al. (2008) or Teflon layer Zhang et al. (2016) inclusion. Due to low energy and non-ionizing character of the THz waves, the method can be applied for delicate materials like leaves or tissues.

The internal structure of the samples was examined using THz spectrometer (TPS Spectra 300 THz Pulsed Imaging and Spectroscopy from TerraView) in reflection mode. The measuring heads were arranged in an angle of 22° between them. During scanning process the measurement step was equal to 0.1 mm and THz signals were registered with tenfold averaging. During measurements the sample was put on a metal table that surface was parallel to the spectrometer's heads.

Comparison of THz scans for the same sample after manufacturing and after the thermal loading are presented in Figures 5-7.

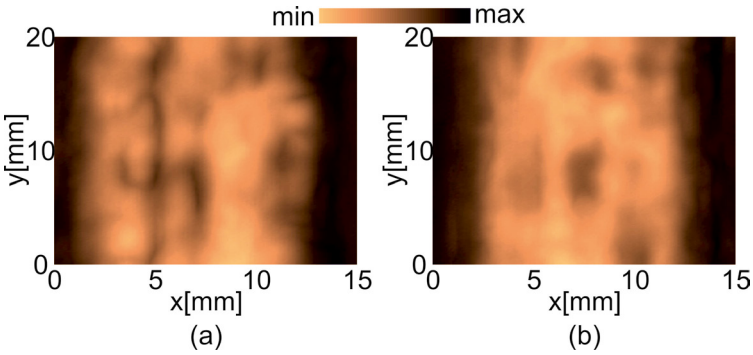


Fig. 5. Comparison of C-scans for surface of sample: (a) after manufacturing, (b) after the thermal loading.

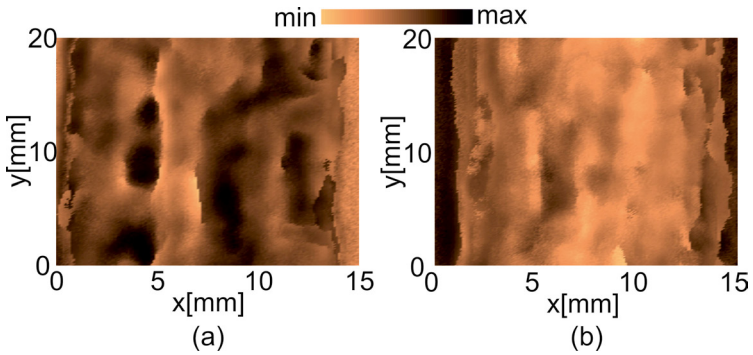


Fig. 6. Comparison of C-scans for the plane with embedded FBG sensor: (a) after manufacturing, (b) after the thermal loading.

The presented THz maps shows differences in internal structure of material due to the temperature and moisture influence. The surface pattern (parallel glass fibres) is not visible for the sample after manufacturing (Figure 5(a)). Probably it is an influence of PLA layer covering fibres. Thermal treatment results in separating the glass fibre bundles and air occurrence between them (Figure 5(a)). Due to this it is possible to see the parallel glass fibre bundles.

The next analysed plane, was the plane where FBG sensor was embedded. Fibre optic is not covered by PLA as, on contrary to glass fibres, it was not prepared for 3D printing. It is well visible for the sample after manufacturing (Figure 6(a)). Temperature and moisture affects the internal structure and increase the PLA connection with optical fibre (Figure 6(b)). Optical fibre and glass fibre parameters (refractive index, absorption coefficient) are similar for THz waves. In the GFRP material, the main difference between them was related to PLA layer. Therefore, after the thermal loading influence, optical fibre is less recognisable than before.

During the THz measurements, the samples were laying on a metal plate. It results in total reflection of the THz wave. Due to this the glass bundles pattern is well visible for the intact sample (Figure 7(a)). There are also visible some voids in connections between the glass reinforcements. Moisture and temperature influenced the internal structure of the sample (Figure 7(b)).

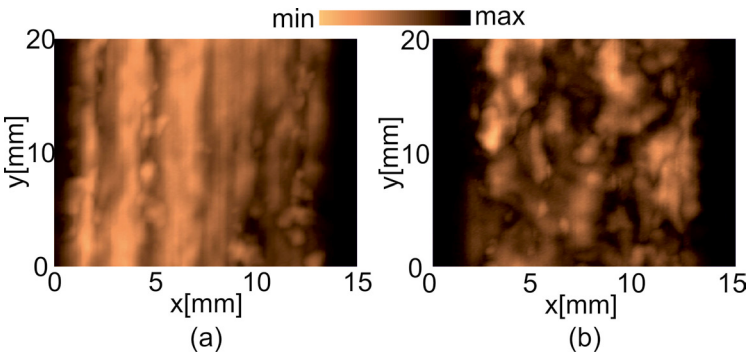


Fig. 7. Comparison of C-scans for the bottom surface of the sample: (a) after manufacturing, (b) after the thermal loading.

### *3.3. Tensile test*

The samples (after manufacturing and after the thermal treatment) were subjected to the tensile test. Its aim was to determine the embedded fibre optic as well as the temperature loading and moisture influences on the GFRP material durability. The tensile tests were performed on universal static-dynamic testing machine HT-9711-25 (Hung Ta, Korea).

The averaged tensile strength of the samples was ca. 210 MPa with maximal difference 5% regardless the thermal treatment or the FBG sensors occurrence. The maximal strain value for samples with embedded optical fibres is higher 9% than for samples without an FBG sensor. It can be concluded that the FBG sensor influence on the GFRP material is very limited. An example of stress-strain relationship measured by the tensile machine is presented in Figure 8. For all cases, the degradation process is observed as decreasing of the force under stable strain values. When the load value is smaller than 50% than the maximal value the tensile test is automatically stopped.

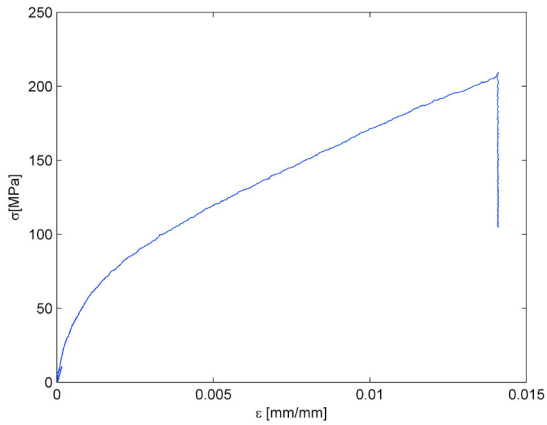


Fig. 8. Samples after the tensile test: (a) after manufacturing, (b) after the thermal loading.

The fracture process of the AM GFRP structures was not typical. Instead of a standard breaking of fibre reinforcement, debonding between neighbouring glass fibre bundles and pulling out the fibres was observed. In samples after manufacturing, the pulling out process is observed for selected fibre bundles. For samples after thermal loading the process is observed for almost all fibre bundles. Photographs from optical microscope presenting the comparison between samples are presented in Figure 9.

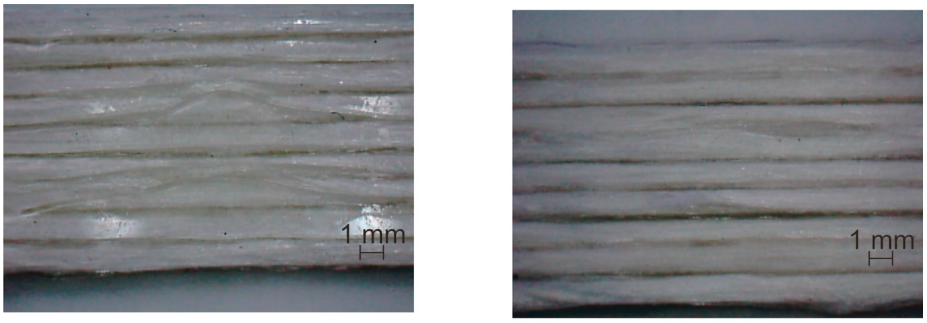


Fig. 9. Samples after the tensile test: (a) after manufacturing, (b) after the thermal loading.

## 4. Conclusion

The paper presents GFRP samples manufactured using FDM method. The samples were divided into two groups: without and with embedded FBG sensors.Embedding process does not influenced the FBG spectra shapes. However, the structure of the sample contains connected glass fibre bundles. It is not possible to distinguish glass fibre and PLA matrix.

Samples from both groups were then exposed to elevated temperature under stable RH values (20% and 95%). The fibres preparation resulted in lower glass transition of PLA. Also, moisture influence was visible as decreasing the glass transition temperature of PLA and strain values.

Both sample types were subjected to the tensile test. Regardless of the embedded sensors and temperature loading, the strain-stress characteristics were similar. Also, the degradation process was almost the same and based on spiting glass fibres bundles and pulling out separate fibres.

## 5. Acknowledgment

This research was supported by the project entitled 'Additive manufactured composite smart structures with embedded fiber Bragg grating sensors (AMCSS)' funded by the National Science Centre, Poland under M-ERA.NET 2 Call 2019, grant agreement 2019/01/Y/ST8/00075.

## References

Chen, J., Wang, J., Li, X., Sun, L., Li, S., Ding, A., 2020. Monitoring of temperature and cure-induced strain gradient in laminated composite plate with fbg sensors. Composite Structures 242, 112168.

Cristea, M., Ionita, D., Iftime, M.M., 2020. Dynamic mechanical analysis investigations of pla-based renewable materials: How are they useful? Materials 13, 5302.

Cucinotta, F., Guglielmino, E., Sfravara, F., 2017. Life cycle assessment in yacht industry: A case study of comparison between hand lay-up and vacuum infusion. Journal of Cleaner Production 142, 3822–3833.

Dickson, A.N., Barry, J.N., McDonnell, K.A., Dowling, D.P., 2017. Fabrication of continuous carbon, glass and kevlar fibre reinforced polymer composites using additive manufacturing. Additive Manufacturing 16, 146–152.

Eftekhari, M., Fatemi, A., 2016. Tensile behavior of thermoplastic composites including temperature, moisture, and hygrothermal effects. Polymer Testing 51, 151–164.

Eslami, S., Taheri-Behrooz, F., Taheri, F., 2012. Effects of aging temperature on moisture absorption of perforated gfrp. Advances in Materials Science and Engineering 2012.

Feng, P., Meng, X., Chen, J.F., Ye, L., 2019. Mechanical properties of structures 3d-printed with cementitious powders, in: 3D Concrete Printing Technology. Elsevier, pp. 181–209.

Gebremichael, Y., Li, W., Boyle, W., Meggitt, B., Grattan, K., McKinley, B., Fernando, G., Kister, G., Winter, D., Canning, L., et al., 2005. Integration and assessment of fibre bragg grating sensors in an all-fibre reinforced polymer composite road bridge. Sensors and Actuators A: Physical 118, 78–85.

Karaş, B., Smith, P.J., Fairclough, J.P.A., Mumtaz, K., 2022. Additive manufacturing of high density carbon fibre reinforced polymer composites. Additive Manufacturing 58, 103044.

Mieloszyk, M., Andrearczyk, A., Majewska, K., Jurek, M., Ostachowicz, W., 2020. Polymeric structure with embedded fiber bragg grating sensor manufactured using multi-jet printing method. Measurement 166, 108229.

Muna, I.I., Mieloszyk, M., 2021. Temperature influence on additive manufactured carbon fiber reinforced polymer composites. Materials 14, 6413.

Nagulapally, P., Shamsuddoha, M., Herath, T., Djukic, L., Prusty, G.B., 2023. Mechanical and optical performance evaluations of embedded polyimide and peek coated distributed optical sensors in glass fibre reinforced composites with vinyl ester resin systems. Journal of Composite Materials 57, 1707–1728.

Park, S., Park, T., Han, K., 2011. Real-time monitoring of composite wind turbine blades using fiber bragg grating sensors. Advanced Composite Materials 20, 39–51.

Rimašauskas, M., Kuncius, T., Rimašauskienė, R., 2019. Processing of carbon fiber for 3d printed continuous composite structures. Materials and Manufacturing Processes 34, 1528–1536.

Roberts, G.W., Hancock, C.M., Lienhart, W., Klug, F., Zuzek, N., de Ligt, H., 2021. Displacement and frequency response measurements of a ship using gps and fibre optic-based sensors. Applied Geomatics 13, 51–61.

Sá, M.F., Guerreiro, L., Gomes, A.M., Correia, J.R., Silvestre, N., 2017. Dynamic behaviour of a gfrp-steel hybrid pedestrian bridge in serviceability conditions. part 1: Experimental study. Thin-Walled Structures 117, 332–342.

Stoik, C.D., Bohn, M.J., Blackshire, J.L., 2008. Nondestructive evaluation of aircraft composites using transmissive terahertz time domain spectroscopy. Optics express 16, 17039–17051.

Tuwair, H., Volz, J., ElGawady, M., Mohamed, M., Chandrashekhara, K., Birman, V., 2016. Behavior of gfrp bridge deck panels infilled with polyurethane foam under various environmental exposure, in: Structures, Elsevier. pp. 141–151.

Vaggar, G.B., Kamate, S., Badyankal, P., et al., 2018. Thermal properties characterization of glass fiber hybrid polymer composite materials. Int. J. Eng. Technol 7, 455–458.

Wu, B., Wu, G., Yang, C., 2019. Parametric study of a rapid bridge assessment method using distributed macro-strain influence envelope line. Mech. Syst. Signal Process. 120, 642–663.

Zhang, J., Wang, J., Han, X., Cui, H.L., Shi, C., Zhang, J., Shen, Y., 2016. Noncontact detection of teflon inclusions in glass-fiber-reinforced polymer composites using terahertz imaging. Applied Optics 55, 10215–10222.